PHENOMENOLOGICAL MODELING APPROACH TO ANISOTROPIC ABLATION IN MOLTEN CORE CONCRETE INTERACTIONS

Kyoung M. Kang and Michael Corradini*
Department of Nuclear Engineering and Engineering Physics
University of Wisconsin-Madison
1500 Engineering Drive, Madison, WI 53706, USA
*: corradini@engr.wisc.edu

ABSTRACT

As a result of recent molten core-concrete interaction (MCCI) experiments, CCI tests, the trend of concrete ablation consistently depends on the type of concrete. Specifically, tests with LCS concrete yields isotropic concrete ablation in comparison to anisotropic ablation with siliceous concrete. Isotropic ablation means vertical and horizontal ablations depths are similar in each experiment, while anisotropic ablation means ablation into a vertical wall is much greater than ablation to bottom wall. This is an interesting result, since MCCI simulant experiments indicate that there should be only isotropic ablation. Simulation results of CCI tests by the CORQUENCH code, a well-known MCCI computer model, shows good agreement with the cases with isotropic ablation but not with the cases with anisotropic ablation. Thus, the goal of this work is to better understand the reasons for anisotropic ablation in cases with siliceous concrete. One empirically observes a clear separation between melt and concrete, with no solid gravel in the solidified corium for MCCI tests with LCS concrete, while there is solid gravel observed in the solidified corium in cases with siliceous concrete. Given this consistent observation, two physical effects are expected: delayed gas release by the silica gravel and surface area enhancement at the concrete-corium interface. These effects can cause anisotropic ablation in cases with siliceous concrete. This phenomenological approach is modeled and implemented into the CORQUENCH code in this work. Comparison of simulation result of the modified and existing CORQUENCH model for CCI tests for cases with siliceous concrete shows that the modified code has better agreement to test data.

KEYWORDS
Anisotropic ablation, MCCI, Modeling, CCI experiments

1. INTRODUCTION

A postulated severe accident of light water reactors involves melting of fuel rods and structural materials in the core region as a result of prolonged failure of the safety cooling systems. If these materials slump into the reactor vessel lower plenum and debris coolability cannot be achieved in-vessel, core melt would fail the bottom head of reactor vessel and settle on the concrete floor of the containment building (pedestal region in BWR or reactor cavity in PWR). This ex-vessel severe accident scenario is our focus here and is shown conceptually in Fig. 1.

After the relocation of core melt onto the base-mat of the concrete building, the core melt (corium) starts eroding the concrete, because the temperature of the melt is much higher than concrete materials thermal decomposition temperature; i.e., so-called ‘ablation temperature’ since it’s modeled as rapid removal of material from the surface by erosive processes. The ablation of the concrete accompanied by melting of

the cement material, detachment and melting of the aggregate gravel and generation of chemically bound decomposition gases (carbon-dioxide and water vapor). This Molten Corium Concrete Interaction (MCCI) process continues until the core melt has cooled down below this ablation temperature by energy transfer to overlying water cooling and from concrete decomposition into the corium pool. This ablation to concrete cavity walls not only undermines structural integrity of the concrete building, but also might eventually cause penetration of the containment wall resulting in release of radioactive material to surrounding environment. Although this scenario has low probability to occur, ex-vessel severe accident can lead to significant consequences to the public health and environment. Thus, a better understanding of MCCI is necessary for complete safety assessment of light water reactor.

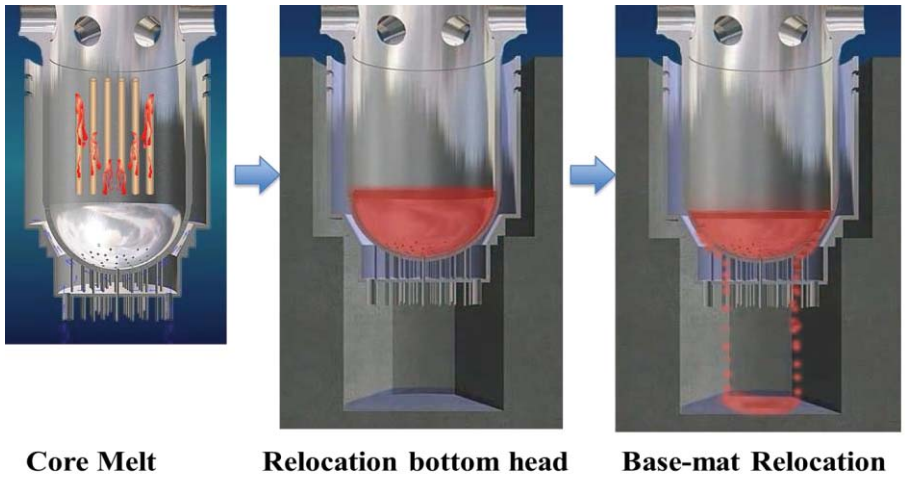

Figure 1. Ex-vessel severe accident scenario.

The Core Concrete Interaction (CCI) tests series has recently been performed in Argonne National Laboratory in United States [1]. The CCI tests are large scale, real material experiments with a cubic concrete geometry and direct electrical heating of the melt to simulate core decay heat. Similar real material, medium scale experiments with a half cylinder concrete geometry and induction heating have been performed at the VULCANO facility in Cadarache, France [2]. The top view and 3-dimensional view of CCI and VULCANO tests shows differences between two tests as illustrated in Fig. 2.

The Limestone and Common Sand (LCS) concrete and Siliceous (SIL) concrete were used for the CCI and VULCANO tests. The ablation trend shown in the experiments strongly depended on the concrete type. The lateral ablation depth was much higher than the axial ablation in both CCI and VULCANO tests, when silica concrete was used in the experiments. On the other hand, lateral and axial ablation was almost identical in the experiments with LCS concrete of CCI and VULCANO tests. Currently there is no mechanistic model to explain this empirically observed anisotropic ablation.

One interesting post-test observation in CCI and VULCANO tests, between isotropic ablation and anisotropic ablation tests, was the existence of solid aggregate gravel in the solidified corium near the interface between the melt and concrete for SIL concrete. This observation is an empirical clue to can explain the anisotropic ablation in cases with SIL concrete. Modeling of underlying phenomena, which was not considered in current MCCI computer models, is performed in this paper. The proposed model is implemented into the MCCI code, CORQUENCH (CORium QUENCHing) code, and prediction of the code with and without the model is compared with CCI tests 2 and 3.

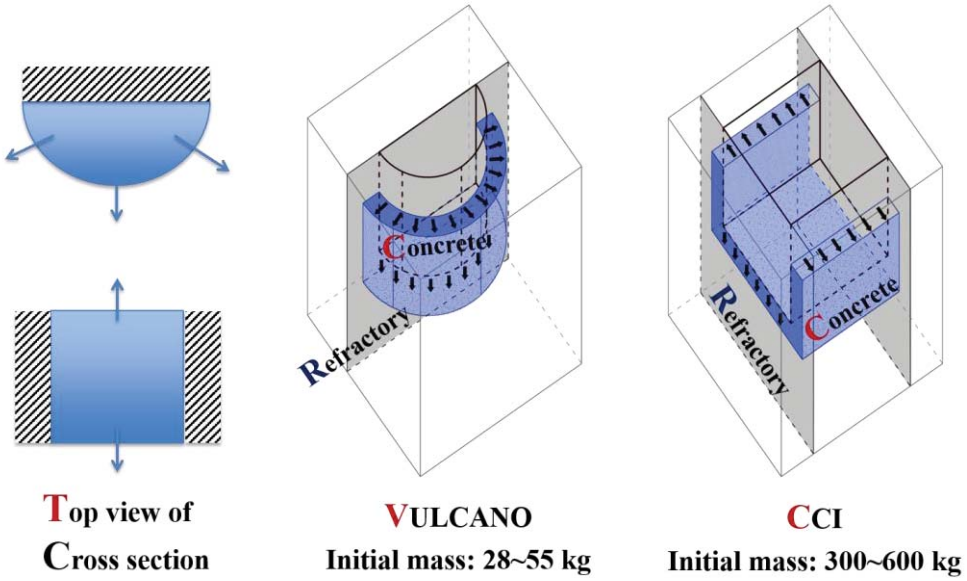

Figure 2. Top view and 3-D view of concrete cavity in VULCANO and CCI tests (the hashed region indicates an insulated boundary for the VULCANO and CCI tests).

2. PREDICTION OF CURRENT CODE

2.1. CCI Tests 2 and 3

Initial and boundary conditions of CCI tests 2 and 3 are summarized in Table I. LCS and SIL concrete are used for CCI tests 2 and 3, respectively. Initial condition and power input is almost identical between two tests. Chemical composition of LCS and SIL concrete is listed in Table II [1].

Table I. Summary of CCI tests 2 and 3

Parameter	CCI tests	
	CCI-2	CCI-3
Concrete type	LCS	SIL
Basemat cross-section	50 cm x 50 cm	
Initial melt mass (depth)	400 kg	375 kg
Initial melt temp. (deg C)	1880	1950
Input power (kW)	120	120
Lateral-axial ablation ratio	**1:1**	**4:1**

Table II. Chemical composition of Concrete

wt%	CCI-2	CCI-3
Al_2O_3	2.49	3.53
CaO	**25.88**	**16.79**
Fe_2O_3	1.39	1.49
MgO	11.47	0.85
SiO_2	**21.61**	**59.91**
CO_2	**29.71**	**9.8**
H_2O	4.37	3.69
Total	96.92	96.06

2.2. CORQUENCH Code

CORQUENCH code was developed as a MCCI code in Argonne National Laboratory as a result of an international research program [3]. This computer model was developed to better model the conditions under which ex-vessel core coolability is achieved when core materials are in contact with an overlying water pool. The CORQUENCH model for heat and mass transfer to concrete walls is based on the CORe CONcrete Mod3 (CORCON-Mod3) code [4], which was developed at Sandia National Laboratories. Thus, the effects of an overlying water pool and modification of several associated models were the key innovations in CORQUENCH. The version of the CORQUENCH code used in this work is 3.04b.

2.3. Comparison of CORQUENCH Simulation with Experiments

The CORQUENCH simulation for CCI-2 and CCI-3 uses the Bradley slag film model, and is presented in the CORQUENCH manual [3]. The CORQUENCH simulation is reproduced by version 3.04b and compared with experimental data. With respect to heat transfer, the ablation depth and melt temperature are two important data, which were measured during the MCCI experiments. Fig. 3 and Fig. 4 show the comparison of the melt temperature and the ablation depth as time between the simulation and the test results for CCI-2 test. The CORQUENCH code predicts the result for the CCI-2 test quite well, which is the case with LCS concrete. Fig. 5 and Fig. 6 illustrate the CORQUENCH simulation result and experimental data of CCI-3 test. In comparison with the simulation result for CCI-2, the result for CCI-3 does not well predict the experimental data particularly erosion depth. Specifically, the CORQUENCH does not show the anisotropic ablation shown in the experiment and over predicts the melt temperature.

2.4. Source of the Observed Anisotropic Ablation

The observed anisotropic ablation seem to be based on the differences between LCS concrete and SIL concrete, since the concrete type is only distinct difference between CCI tests 2 and 3. Based on the result for the real material experiments including CCI and VULCANO tests, Journeau, et al. summarized differences between LCS and SIL concrete [5]. They are: chemical composition and gas mole contents in concrete, decomposition enthalpy, concrete-melt interface with existence of solid aggregate gravel in the solidified corium particularly near the concrete-corium interface, and concrete shrinkage phenomenon.

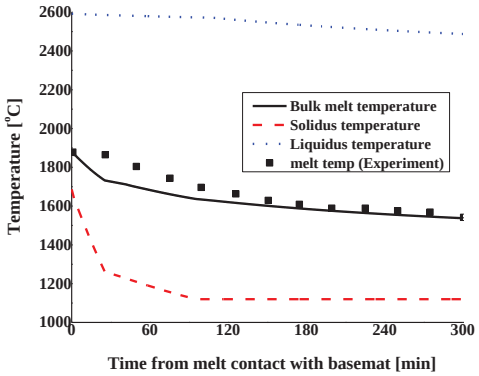

Figure 3. Melt temperature in CORQUENCH simulation for CCI-2.

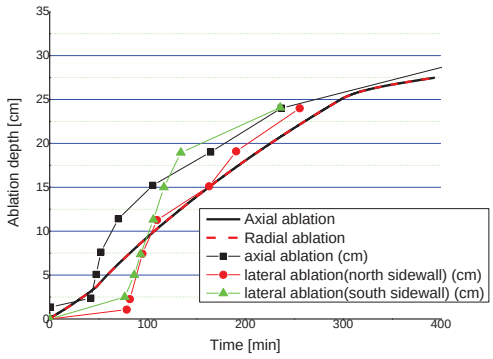

Figure 4. Ablation depth to vertical wall in CORQUENCH simulation for CCI-2.

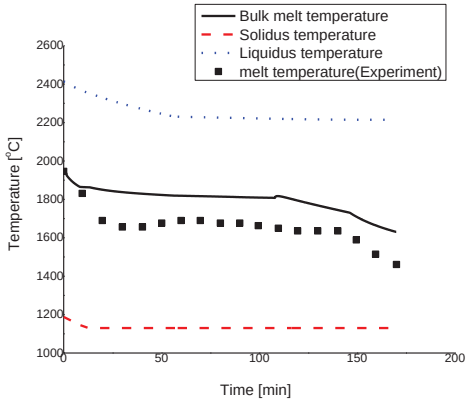

Figure 5. Melt temperature in CORQUENCH simulation for CCI-3.

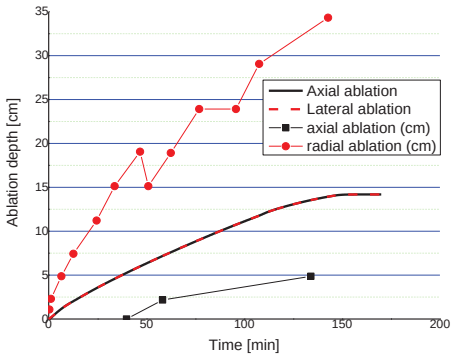

Figure 6. Ablation depth in CORQUENCH simulation for CCI-3.

2.5. Previous Modeling Effort for Anisotropic Ablation

After anisotropic ablation was observed in CCI and VULCANO tests, many researchers have tried to understand the phenomenon, although no mechanistic explanation has been proposed. As a response to the need for code simulation for a case of anisotropic ablation, several researchers developed empirical approaches; i.e., the erosion data was used to develop an empirical relationship from real material experiments without an understanding of the anisotropic heat transfer.

2.5.1. Sevon's correlation

Sevon correlated two variables from the data points of the CCI tests 1-3: the superficial gas velocity and the heat transfer coefficient [6]. His correlations are as following:

$$h = 2906v_g + 49 \text{ at the basemat for all type concretes} \quad (1)$$

$$h = 5736v_g + 26 \text{ at sidewall for siliceous concrete} \quad (2)$$

$$h = 3206v_g + 57 \text{ at sidewall for limestone and common sand} \quad (3)$$

Although his correlation includes an anisotropic heat transfer, there are several limitations. First of all, he correlates only the superficial gas velocity and the heat transfer coefficient, even though there are many variables that might affect the heat transfer coefficient, so the correlation cannot be applied to the cases with various concrete compositions. Moreover, there is no phenomenological understanding for the source of the anisotropic heat transfer in his correlation.

2.5.2. Anisotropic ratio as an input

TOLBIAC-ICB code was developed as a MCCI computer code by CEA in France [7]. Anisotropic heat transfer is usually the result of the MCCI code rather than the input of the code. However, the ratio of anisotropy can be inserted as an input in the TOLBIAC-ICB code in order to simulate the anisotropy in the MCCI experiment such as observed in VULCANO. The simulation result can well describe the cases with both the siliceous and LCS concrete with a proper anisotropic ratio provided that the ratio has been empirically determined for any given case. The TOLBIAC-ICB code has similar limitations like the Sevon's correlation. Although it includes the anisotropic heat transfer, it does not have any

phenomenological understanding about anisotropy. In addition, this code is not capable of simulating the MCCI experiment without knowing the anisotropic ratio preemptively.

3. MODEL DEVELOPMENT

3.1. Difference of Concrete Melt Interface with Existence of Unmelted Gravel

Concrete is composed of aggregate (gravel and sand), and neat cement paste (a mixture of hydraulic cement and water). Chemical composition of LCS concrete and SIL concrete are listed in Table II. Main chemical component of gravel is calcium magnesium carbonate ($CaMg(CO_3)_2$) or calcium carbonate ($CaCO_3$) in LCS concrete, and silicon dioxide (SiO_2) in SIL concrete. However, both LCS and SIL concretes have neat cement paste with similar chemical composition. The main chemical composition of neat cement paste is calcium hydroxide ($Ca(OH)_2$). When the temperature of concrete reaches about 1450 K, both LCS gravel and neat cement paste decompose, while SIL gravel aggregate would not decompose at that temperature, but rather at a higher temperature of 1870 K. At 1450 K, since neat cement paste loses its bonding ability, SIL gravel can detach from concrete surface without melting and by buoyancy and gas release be transported into the pool as a solid. In contrast, one would expect the LCS gravel to be thermally decomposed and melted at the interface with the neat cement paste. In this conceptual model the sand aggregate has a small size (<<1mm) and small amount and is considered to be homogeneously mixed with the neat cement paste.

Fig. 7 provides the picture of interface between the concrete and the melt by post-test observation of CCI tests [1]. Fig. 7 (a) is the interface of SIL concrete test (CCI-1) and (b) is that of LCS concrete test (CCI-2). In comparison to Fig. 7 (b), many solid pieces of gravel (white spots) are shown near the interface in Fig. 7 (a). In addition, there is gray area which is mixed area between the melt core and the solid concrete in Fig. 7 (a), but the core melt and concrete is clearly separated in Fig. 7 (b).

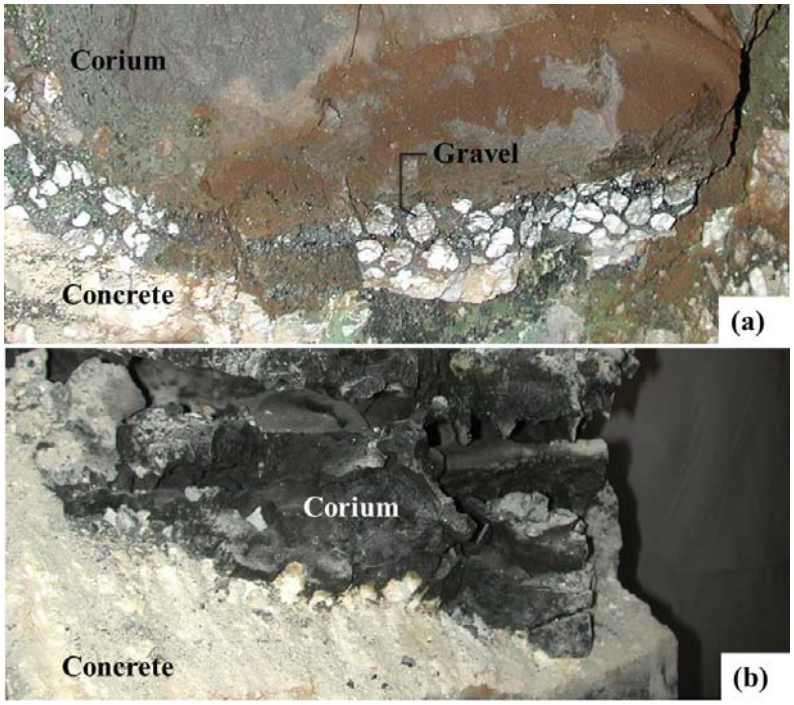

Figure 7. Interface of siliceous concrete and LCS concrete: (a): CCI-1 and (b): CCI-2 [1] (Note the presence of aggregate gravel in the solidified corium near the concrete-corium interface for CCI-1).

3.2. Interfacial Area Enhancement

3.2.1. Phenomenology

A conceptual picture of the thermal decomposition for the two concrete types shows the difference of SIL concrete from that of LCS concrete, as depicted in Fig. 8. Existence of unmelted siliceous gravel effectively increases the interfacial heat transfer area at the interface between corium and concrete. Current model works well for the case of LCS concrete, because limestone gravel is melted with corium contact. However, it does not properly represent the case with SIL concrete, because there would be area augmentation by the unmelted siliceous gravel. This area augmentation would occur for both horizontal and vertical walls.

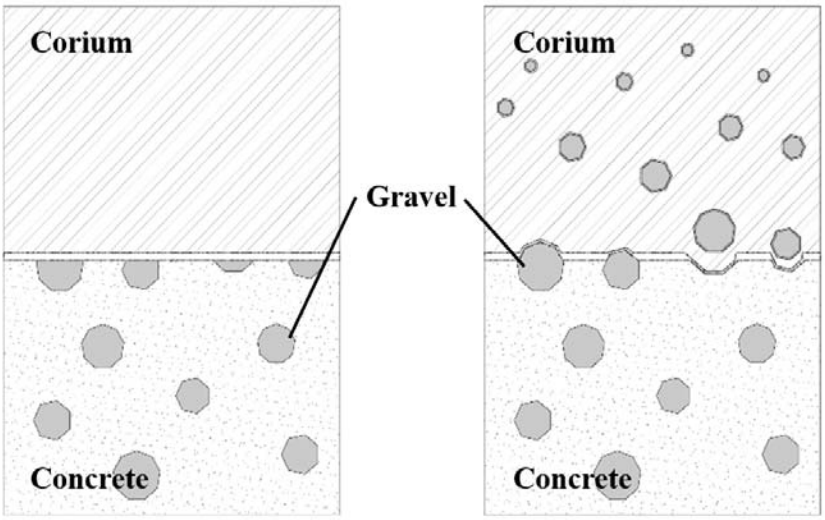

Figure 8. Conceptual drawing of different ablation pattern between LCS and SIL concrete. (Left: LCS, Right: SIL).

3.2.2. Model

Interfacial area enhancement by gas sparging effect at melt water interface is used in the CORQUENCH code [8]. The logic used in that model can be similarly applied to interfacial area enhancement by unmelted SIL gravel as discussed here.

The overall heat transfer coefficient between the melt and concrete of the model is

$$h_{overall} = A^* \times h_{current} \tag{4}$$

where dimensionless interfacial area enhancement, A*, which is the effect of surface area deformation by unmelted gravel, is

$$A^* = \frac{A_{original} + A_{increased}}{A_{original}} \tag{5}$$

$$A^* = 1 + \overline{a^*} \times \dot{n}''_{gravel} \times t_r \tag{6}$$

$\overline{a^*}$ is time average increased area by one gravel particle, $\dot{n}''_{gravel}$ is number of gravel per unit time and area, and t_r is resident time elapsed from contact between corium and gravel to detachment of gravel.

In this model, $\dot{\eta}_{ab}$, ablation rate, is assumed to be constant during t_r, and all gravel in the concrete are assumed to be spheres. $\dot{n}''_{gravel}$ and t_r are

$$\dot{n}''_{gravel} = \frac{\chi_{SIL}\rho_{concrete}\dot{\eta}_{ab}}{\rho_{SIL}V_{gravel}} \tag{7}$$

$$t_r = \frac{2R}{\dot{\eta}_{ab}} \tag{8}$$

where χ_{SIL} is silicon dioxide in gravel weight portion of the concrete. $\overline{a^*}$ is time averaged integral of increased surface area with constant ablation rate:

$$\overline{a^*} = \frac{\int_0^{t_r} A_{sur}dt}{t_r} \tag{9}$$

In our current model to estimate the area enhancement, A*, for LCS concrete and SIL concrete are approximately 1 and 2 by this model, respectively.

3.3. Delayed Gas Release by Silica Gravel

3.3.1. Background

Early investigations of the convection heat transfer during an MCCI, used convection heat transfer experiments in a volumetrically heated water pool as shown in Table III. In many simulant experiments, anisotropic heat transfer was observed (with 2 – 7 anisotropic ratio) in cases without gas injection, while isotropic heat transfer was observed in cases with gas injection. In consideration of simulant experiment result, since there is gas release from decomposition of the concrete in both CCI-2 and 3, heat transfer trend in CCI-2 and 3 should be isotropic. However, as presented in Chapter 2, only CCI-3 test has isotropic heat transfer and CCI-2 has anisotropic heat transfer. Thus, a logical explanation would be that the effect of gas release in CCI-3 is inhibited by the existence of unmelted gravel particles, which is only observed in CCI-3 but not observed in CCI-2.

3.3.2. Phenomenology

The hypothesis of entrapment of the gas in the gravel is that the siliceous gravel would carry the chemically-bound carbon dioxide through the slag layer while being entrapped in the gravel in this process. How gravel particles can carry bound gas is not specifically identified in this research, but Fig. 9 illustrates the assumption of the concept between the current model and the new one in siliceous concrete. In the case for siliceous concrete, all the decomposed gas is released from the concrete ablation front (interface between the slag layer and the concrete) in the current model, whereas some of the decomposed gas passes through the slag layer within gravel and is released in the melt pool in the hypothetical model. If this hypothesis is right, only 30 – 60 % of decomposed gas will contribute to the heat transfer

depending on the concrete composition in the siliceous concrete. However, since most of gravel in LCS concrete thermally decomposes due to de-carbonation at the concrete-pool interface, the decomposed gas is released at that location in both the current model and new model as shown in Fig. 9 (a). Therefore, for the case with the siliceous concrete in the new model, the heat transfer coefficient by the bubble agitation is much smaller and heat transfer via natural convection can be the controlling heat transfer mechanism with the bubble agitation in new model. This natural convection causes 2~7 times higher heat transfer coefficient at the vertical wall than at the horizontal wall based on the result for simulant experiments as mentioned in Chapter 3.3.1.

Table III. Summary of the study of heat transfer with volumetrically heated pool.

References	Heat transfer	Heat Transfer Trend	Anisotropic ratio
Fishenden and Saunders [9]	Natural convection (No gas)	Anisotropy	2
Kulacki and Goldstein [10]	Natural convection (No gas)	Anisotropy	5 – 7
Kulacki, et al. [11]	Natural convection (No gas)	Anisotropy	5 – 7
Jahn and Reineke [12]	Natural convection (No gas)	Anisotropy	4 – 5
Felde, et al. [13]	Convection with gas injection	Isotropy	1
Journeau and Haquet [14]	Convection with gas injection	Isotropy	1

3.3.3 Model

Bradley slag film model is currently used for the simulation of the CORQUENCH code [3]. In an assumption of quasi-steady concrete erosion, the gas generation rate at the core-concrete interface is:

$$j = \frac{\chi_{gas}\rho_{con}\dot{\eta}_{ab}}{\rho_{gas}} \tag{11}$$

where j is superficial gas velocity, $\dot{\eta}_{ab}$ is ablation rate, and χ_{gas} is gas mass content of the concrete.

However, because the gas within the gravel passes through the core-concrete interface in this model, effective gas generation rate, j_{eff}, which contributes to heat transfer in Bradley's model, might be:

$$j_{eff} = \frac{(\chi_{gas} - \chi_{gas\ in\ gravels})\rho_{con}\dot{\eta}_{ab}}{\rho_{gas}} \quad (12)$$

where $\chi_{gas\ in\ gravel}$ is gas mass content in the gravel. j_{eff} from equation (12) is about a half of j by this model from equation (11) in CCI-3, while j_{eff} is same with j in CCI-2.

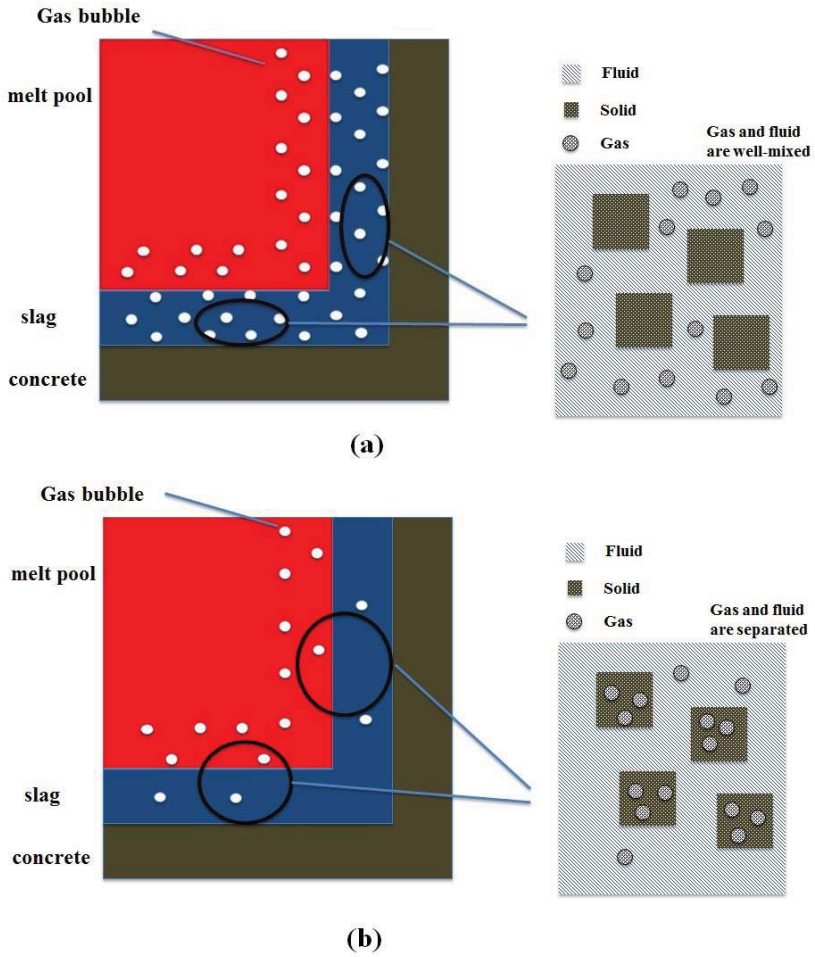

Figure 9. Conceptual drawing of the gas entrapment in the gravel: (a) current model and (b) new hypothetical model.

4. COMPARISON WITH EXPERIMENTS

The proposed model was implemented into the CORQUENCH code. The prediction by the modified code and original code are compared with experimental result together. Input and boundary conditions of simulation by both original and modified code are identical based on the information provided in the CORQUENCH manual [3]. Because our model is based on the silica content in the concrete, there is no difference between the result by modified and original code, since limestone gravel and neat cement paste in CCI-2 melts at the ablation front together. However, simulation of modified and original code of CCI-3 yields different results.

The result of the CORQUENCH simulation for CCI-3 with the current and modified model is provided in Fig. 10 and Fig. 11. The anisotropic ablation is described in the modified model in contrast to the result of the current model as shown in Fig. 10, so the prediction approaches the experimental data much closer in the modified model than in the current model. In addition to the anisotropic ablation, the melt temperature is also predicted closer to the experimental data in the modified model than the current model.

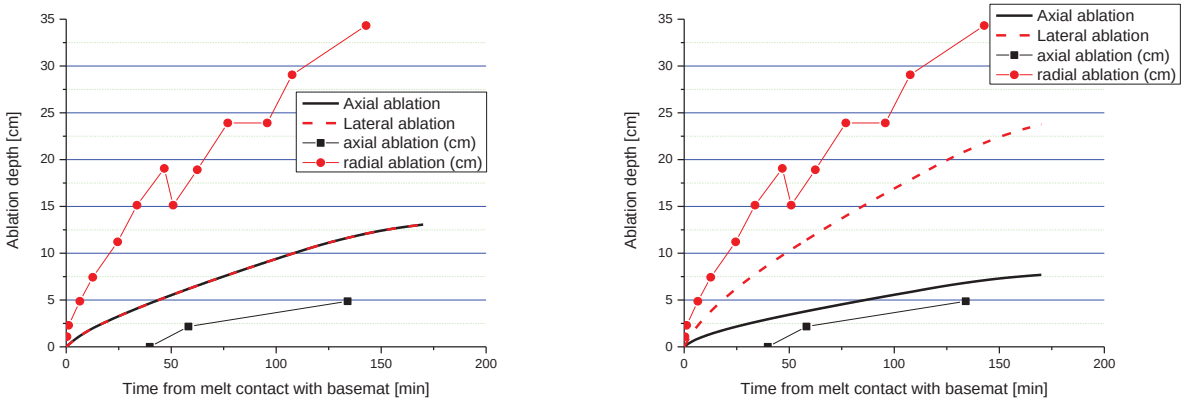

Figure 10. Ablation depth in CORQUENCH simulation for CCI-3 test (Left: current model, Right: modified model).

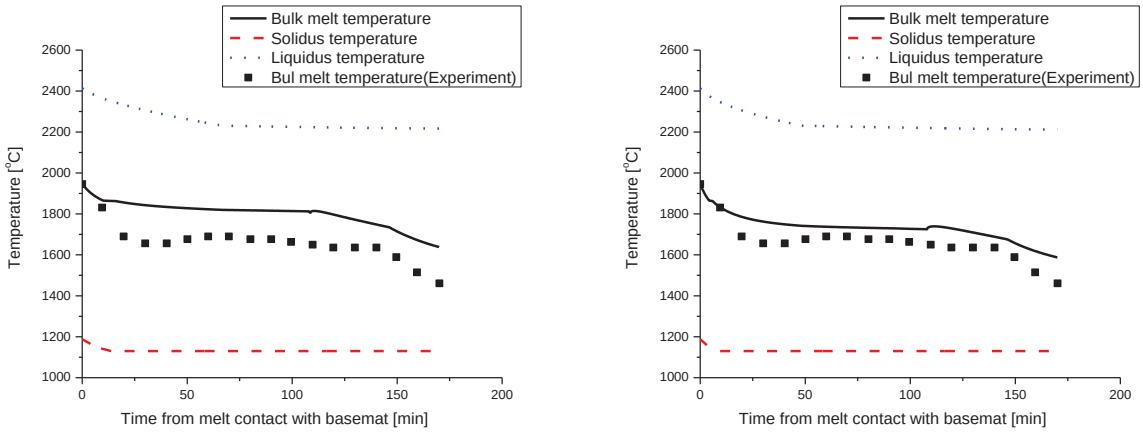

Figure 11. Melt temperature in CORQUENCH simulation for CCI-3 test (Left: current model, Right: modified model).

5. SUMMARY AND CONCLUSION

Anisotropic ablation, which has higher ablation rate for vertical concrete wall erosion than to horizontal bottom wall erosion, is observed in real material MCCI experiments with SIL concrete, whereas isotropic ablation is found in the experiments with LCS concrete. Other input or boundary conditions do not seem to be the cause of this different result. The CORQUENCH code can predict the LCS case with isotropic ablation, but cannot predict the observed anisotropic ablation. Although there are several empirical approaches to explain this different ablation pattern, there is currently no mechanistic model for this phenomenon.

Several observed differences between LCS and SIL concrete suggest a reason for this anisotropic ablation. A different interface between corium and concrete, with the existence of solid silica aggregate gravel in the solidified corium is the most important one of those differences found in post-test observation of CCI and VULCANO tests. Effects of this phenomenon to heat transfer between the corium and concrete are envisioned as an effective interfacial heat transfer area enhancement and a delayed gas release by the silica gravel. They are modeled and implemented into CORQUENCH code.

Based on these phenomena, we modified the original CORQUENCH code simulation and compared the simulation with experimental result for CCI tests 2 and 3. The modified code does not alter the results for CCI-2, which is the case of isotropic ablation. However, CCI-3, which is the case of anisotropic ablation, is predicted to be in better agreement with the experimental data.

The current interfacial area enhancement model assumes heat transfer increase with gravel particles and is proportional to increased area of the gravel. The unmelted gravel enhances not only the circulation to the flow but also the instability of the slag layer. Both effects can enhance the heat transfer rate, and the simulation can better predict test data.

The phenomenological modeling used in this work is based on a working hypothesis. It provides a logical explanation as well as better prediction to anisotropic and isotropic ablation found in CCI tests. More analysis is underway to validate this phenomenological model using other MCCI real material experiments such as other CCI tests and VULCANO tests.

NOMENCLATURE

$\dot{\eta}$ = Ablation rate
ρ = Density
χ = Weight portion
$\overline{a^*}$ = Time averaged increased area by one gravel
A^* = Dimensionless interfacial area enhancement
h = Heat transfer coefficient
j = superficial gas velocity
$\dot{n}''$ = Number of generated gravel per time and area
R = Radius
t = Time
V = Volume

ACKNOWLEDGMENTS

Support for this work was provided through the U.S. Nuclear Regulatory Commission. Dr. Mitch Farmer in Argonne National Laboratory presented valuable insights about CCI tests and CORQUENCH code.

REFERENCES

1. M.T. Farmer, S. Lomperski, D.J. Kilsdonk, R.W. Aeschlimann, and S. Basu, *2-D Core Concrete Interaction (CCI) Tests: Final Report*, Argonne National Laboratory Report, OECD/MCCI-2005-TR05, USA (2006).
2. C. Journeau, et al., "Contributions of the VULCANO Experimental Programme to the Understanding of MCCI Phenomena," *Nuclear Engineering and Technology*, **Vol. 44**, pp. 261-272 (2012).
3. M.T. Farmer, *The CORQUENCH Code for Modeling of Ex-vessel Corium Coolability under Top Flooding Conditions,* Chapters 2 and Appendix C, Argonne National Laboratory Report, OECD/MCCI 2010-TR03, USA (2010).
4. D.R. Bradley, et al., *CORCON-MOD3: An Integrated Computer Model for Analysis of Molten Core-Concrete Interactions*, Chapter 2, Sandia National Laboratories Report, NEREG/CR-5843, SAND92-0167, USA (1993).
5. C. Journeau, J.F. Haquet, P. Piluso, and J.M. Bonnet, "Differences between Silica and Limestone Concretes that may Affect Their Interaction with Corium," *Proceedings of 2008 International Congress on Advances in Nuclear Power Plants (ICAPP),* Anaheim, California, USA, June 8-12, 2008 (2008).
6. T. Sevon, "A Heat Transfer Analysis of the CCI Experiments 1-3," *Nuclear Engineering and Design,* **Vol. 238**, pp. 2377-2386 (2008).
7. B. Spindler, B. Tourniarire, and J.M. Seiler, "Simulation of MCCI with the TOLBIAC-ICB Code Based on the Phase Segregation Model," *Nuclear Engineering and Design,* **Vol. 236**, pp. 2264-2270 (2006).
8. M.T. Farmer, J. Sienicki, and B. Spencer, "CORQUENCH: A Model for Gas Sparging-Enhanced, Melt-Water, Film Boiling Heat Transfer," *Proceedings of American Nuclear Society Winter Meeting,* Washington, D.C., USA, November 11-15, 1990, pp. 35-41 (1990).
9. M. Fishenden, and O.A. Saunders, *An Introduction to Heat and Mass Transfer*, Chapter 9, 5th ed., John Wiley, Hoboken, NJ, USA (1950).
10. F.A. Kulacki, and R.J. Goldstein, "Thermal Convection in a horizontal fluid layer with uniform volumetric energy sources," *J. Fluid Mech*., **Vol 55**, part 2, pp. 271-287 (1972).
11. F.A. Kulacki, et al., "Natural Convection With Internal Energy Sources: Some Recent Experimental and Numerical Results with Post-Accident Heat Removal Applications," *Proceedings of the Third PAHR Information Exchange*, ANL-78-10, Argonne National Laboratory, Lemont IL, USA (1977)
12. M. Jahn, and H.H. Reineke, "Free Convection Heat Transfer with Internal Heat Sources Calculations and Measurements," *Proceedings of the Fifth International Heat Transfer Conference*, Tokyo, Japan, septermber (1974).
13. D.K. Felde, H.S. Kim, and S.I. Abdel-Khalik, "Convective Heat Transfer Correlations for Molten Core Debris Pools Growing in Concrete," *Nuclear Engineering and Design*, **Vol. 58.**, pp 65-74 (1980).
14. C. Journeau, J-F, Haquet, "Covection Heat Transfer Anisotropy in a Bubbling Viscous Pool - Application to Molten Core-Concrete Interaction," *Nuclear Engineering and Design*, **Vol 239**, pp 389-394 (2009).